Preparation of nano-structured crystalline tungsten(VI) oxide and enhanced photocatalytic activity for decomposition of organic compounds under visible light irradiation†

Masahiro Sadakane,* Keisuke Sasaki, Hironobu Kunioku, Bunsho Ohtani, Wataru Ueda and Ryu Abe*

Received (in Cambridge, UK) 1st September 2008, Accepted 17th October 2008
First published as an Advance Article on the web 17th November 2008
DOI: 10.1039/b815214d

Nano-structured crystalline tungsten(VI) oxides (WO_3) were prepared using a colloidal crystal template method; these materials have increased specific surface area compared to crystalline WO_3 prepared without the template, and after platinum loading they show enhanced photocatalytic activity for acetic acid decomposition under visible light.

Titanium(IV) oxide (TiO_2) is widely used as a photocatalyst, displaying excellent activity under ultraviolet (UV) light for a number of industrially useful reactions.[1] However, TiO_2 is not photoactive at visible wavelengths, which is desirable for the efficient decomposition of environmental organic contaminants using sunlight or indoor fluorescent light.[2] Recently, Abe *et al.* reported that crystalline tungsten(VI) oxide (WO_3) loaded with nanoparticulate platinum (Pt) exhibits high photocatalytic activity for the decomposition of organic compounds under visible light.[3] With further refinement of the WO_3 catalyst, it is expected that even higher activity can be achieved. In general, high photocatalytic activity requires both high crystallinity, *i.e.*, lower density of lattice defects to reduce recombination of the photoexcited electrons and holes intended for participation in the catalytic reaction, and high specific surface area to increase the density of active surface sites at which the catalytic reaction can take place.[4] However, in practice, these two preconditions are difficult to satisfy simultaneously using conventional preparation processes for metal oxides, since conversion of the oxide precursor into a highly crystalline catalytic material requires calcination at high temperature, which often results in a reduction in specific surface area. Conventional preparations for WO_3 follow this pattern, with highly crystalline WO_3 usually having a low specific surface area ($<1\ m^2\ g^{-1}$).

In the present study, three-dimensionally ordered macroporous (3DOM) WO_3 is successfully prepared by a colloidal crystal templating method, and the resultant material is shown to exhibit both high crystallinity and high specific surface area compared to the corresponding material prepared without a template. When loaded with Pt as a cocatalyst, the 3DOM WO_3 displays enhanced photocatalytic activity for the decomposition of acetic acid under visible light. The material displaying the highest activity for this reaction is found to be a nano-crystalline form produced by sintering-induced disassembly of the 3DOM-structured WO_3.

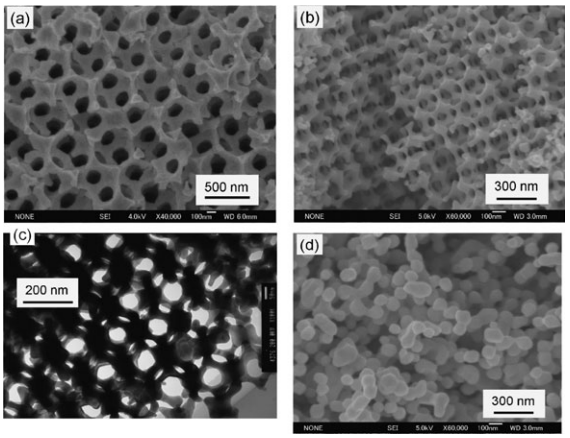

Fig. 1 SEM (a,b,d) and TEM (c) images of WO_3 prepared using a colloidal crystal template. (a) PMMA diameter, 490 nm; calcination temperature, 773 K. (b,c) 180 nm; 773 K. (d) 180 nm, 873 K.

3DOM WO_3 was prepared using a colloidal crystal template (face-centered close-packed array) of mono-disperse poly(methyl methacrylate) (PMMA) spheres prepared by a published method.[5] 3DOM WO_3 materials prepared from tungsten(V) ethoxide[6] and tungsten(VI) chloride[7] as tungsten sources have been reported previously, although the resultant materials had either a poorly ordered pore structure[6] or low pore fraction.[7] In the present study, air-stable and inexpensive ammonium metatungstate ($(NH_4)_6H_2W_{12}O_{40}$) was found to be suitable for the synthesis of 3DOM WO_3, and to afford a well-ordered product. Ammonium metatungstate solution[8] was infiltrated into the voids of the colloidal template and the resulting solid was then calcined at 773 K in a tube furnace under air flow according to the method of Sadakane.[9] This procedure yields well-ordered 3DOM WO_3. Fig. 1 shows scanning electron microscopy (SEM) and transmission electron microscopy (TEM) images of 3DOM WO_3 samples prepared using PMMA spheres of various diameters. More than 90% of the particles identified in the SEM and TEM images display a highly ordered 3DOM structure. The structural data are summarized in Table 1. Treatment at 873 K caused the structure of the 3DOM WO_3 materials with smaller pore diameters to collapse due to sintering (Fig. 1(d)), whereas the 3DOM structure in the material with largest pore size was stable at 873 K (entry 11).

Catalysis Research Center, Hokkaido University, N-21, W-10, Sapporo, 001-0021, Japan. E-mail: sadakane@cat.hokudai.ac.jp; ryu-abe@cat.hokudai.ac.jp; Fax: +81 11-706-9163; +81 11-706-9129; Tel: +81-11-706-9166

† Electronic supplementary information (ESI) available: Powder XRD and Raman spectra of 3DOM WO_3, SEM and TEM images of WO_3 prepared without the template, UV-Vis spectra of 3DOM WO_3 and TEM images of nanocrystalline WO_3. See DOI: 10.1039/b815214d

Table 1 Structural data

Entry	Calc. temp./K	Specific surface area[a]/m^2 g^{-1}	Pore size[b]/nm	Window size[b]/nm	Crystal system
	PMMA (180 nm)				
1	673	28	170	62 × 59	Orthorhombic + monoclinic
2	773	21	166	85 × 69	Monoclinic
3	873	11	[c]	[c]	Monoclinic
4	973	4	[c]	[c]	Monoclinic
	PMMA (260 nm)				
5	673	20	178	68 × 51	Orthorhombic + monoclinic
6	773	15	186	69 × 55	Monoclinic
7	873	12	[c]	[c]	Monoclinic
8	973	8	[c]	[c]	Monoclinic
	PMMA (490 nm)				
9	673	13	430	122 × 101	Orthorhombic + monoclinic
10	773	9	439	150 × 125	Monoclinic
11	873	7	444	168 × 135	Monoclinic
12	973	6	[c]	[c]	Monoclinic
	Without PMMA				
13	773	1	—	—	Monoclinic

[a] BET method. [b] Average of 20 measurements from TEM images.[7] [c] 3DOM structure collapsed due to sintering.

Powder X-ray diffraction (XRD) analysis and Raman spectroscopy revealed that a mixture of orthorhombic (JCPDS 20-1324) and monoclinic (JCPDS 43-1035) WO_3 was formed by calcination at 673 K (entries 1, 5, and 9), whereas pure monoclinic WO_3 was formed at higher calcination temperatures (Fig. S1, S2†).[10]

WO_3 prepared without the PMMA colloidal crystal template grew to particle sizes of up to several micrometers (Fig. S3†) and displayed very low specific surface areas (*ca.* 1 m^2 g^{-1}) (entry 13).[11] In contrast, the specific surface area of the 3DOM WO_3 with pore size of *ca.* 439 nm (entry 10) was 9 m^2 g^{-1}. Even higher specific surface areas of 15 and 21 m^2 g^{-1} were realized at the smaller pore sizes of 186 and 166 nm, respectively. The calculated specific surface areas *ca.* 5, 13, and 14 m^2 g^{-1} for 3DOM WO_3 with 439, 186, and 166 nm macropore diameters, respectively, are similar to the observed specific surface areas.[12] Fig. 2 shows a TEM image and corresponding electron diffraction (ED) patterns for 3DOM WO_3 prepared using PMMA with a diameter of 260 nm. Crystalline 3DOM materials have a skeleton structure consisting of strut-like bonds and vertices, where the struts connect two kinds of vertices.[9] These two kinds of vertex can be seen in Fig. 2: 8-coordinated square prism vertices in zones 4 and 6, and 4-coordinated tetrahedral vertices in zones 2, 3, and 5. Previously, 3DOM crystalline metal oxide materials have been constructed by a connection of smaller crystallites rather than a 3DOM skeleton.[7,9] Therefore, the specific surface area of materials produced in previous syntheses generally has not increased dramatically by producing the 3DOM structure, since the specific surface area is determined not by the macropore diameter but by the crystallite size. In the present case, the whole particle found in zone 1 (Fig. 2) is a single WO_3 crystallite (ED patterns in zone 1–5 are same) which grows around the macropores and connects to an adjacent crystallite in zone 6.

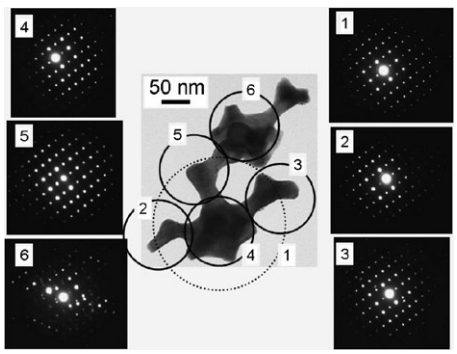

Fig. 2 TEM image (center) and selected-area ED patterns (left, right) of WO_3 prepared using 260 nm PMMA (calcination temperature, 773 K). Zones indicated by 1–6 are selected areas.

Although the formation of mesopores in single crystals has been reported for niobium-based oxides,[13] the present structure appears to be the first example of single crystals growing around macropores. This structure exhibits a markedly higher specific surface area compared to the corresponding non-template material.

The performance of the present materials for the photocatalytic decomposition of acetic acid was evaluated after loading the WO_3 samples with Pt as a cocatalyst. Loading was performed by photodeposition from $H_2PtCl_6{\cdot}6H_2O$ under visible light, first in pure water and then subsequently in aqueous methanol (10 vol%) solution.[3] Fig. 3 plots the generation of CO_2 during gas-phase decomposition of acetic acid over Pt-loaded 3DOM WO_3 and the corresponding catalyst prepared without the PMMA template (all prepared using a calcination temperature

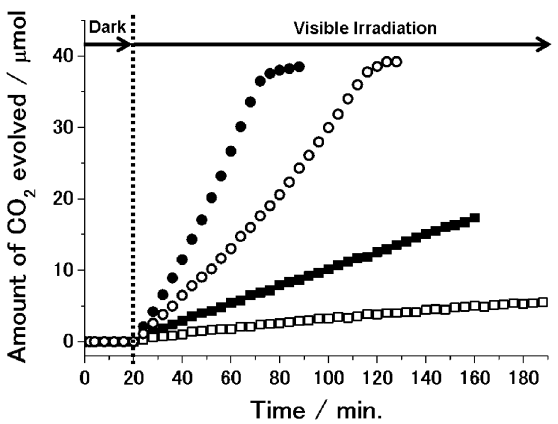

Fig. 3 Time course of CO_2 evolution over Pt-loaded WO_3 prepared using PMMA with a diameter of 180 nm (closed circles), 260 nm (open circles), and 490 nm (closed squares), and over the corresponding material prepared without the template (open squares).

of 773 K).‡ CO_2 generation was observed immediately upon irradiation for all samples, without an appreciable induction time. The rate of CO_2 generation by the samples with the 3DOM structure is considerably higher than that for the corresponding non-template sample, and amongst the 3DOM samples the generation rate increases with decreasing pore diameter. The activity achieved by the Pt-loaded 3DOM WO_3 sample prepared using a 180 nm PMMA template (48 μmol h^{-1}) is higher than that reported previously for a fine Pt-loaded WO_3 particulate (26 μmol h^{-1}; diameter, 50–200 nm; specific surface area, *ca.* 11 m^2 g^{-1}) prepared by centrifugation separation.[3]

Fig. 4 plots the rates of CO_2 generation and the specific surface areas against calcination temperature for the 3DOM WO_3 materials prepared using 180 nm PMMA. With increasing calcination temperature, the specific surface area decreases due to sintering of the WO_3. However, the CO_2 generation rate continues to increase up to a calcination temperature of 873 K, above which the activity decreases slightly. Calcination at such high temperatures reduces the density of impurities, thereby increasing the photocatalytic activity of the final material. Ultraviolet–visible spectroscopy indicates that WO_3 calcined at lower than 873 K contains nitrogen- or carbon-based impurities (shoulder at *ca.*, 510 nm, Fig. S4†). The presence of these impurity elements was also confirmed by a quantitative elemental analysis (data not shown). Calcination at 873 K or higher is required in order to ensure the absence of these impurities, which can cause crystal structure defects that can act as sites for the recombination of photoexcited electrons and holes. The consumption of photogenerated carriers by recombination at defect sites is one of the most important mechanisms of catalyst deactivation.[4a]

The sample exhibiting the highest activity for the decomposition of acetic acid in the present study, WO_3 prepared using 180 nm PMMA and calcined at 873 K, was found to consist of nanoparticles of 80–200 nm in diameter (Fig. 1(d), S5†). This particle diameter is similar to that estimated from the specific surface area.[11] The nanoparticles can be understood to be produced by the sintering-induced disassembly of WO_3 crystals from the 3DOM structure. It has been reported that silica nano-particles are similarly formed by disassembly of 3DOM structures.[14] The present results thus indicate that the 3DOM material is a good precursor for the formation of nanoparticulate materials.

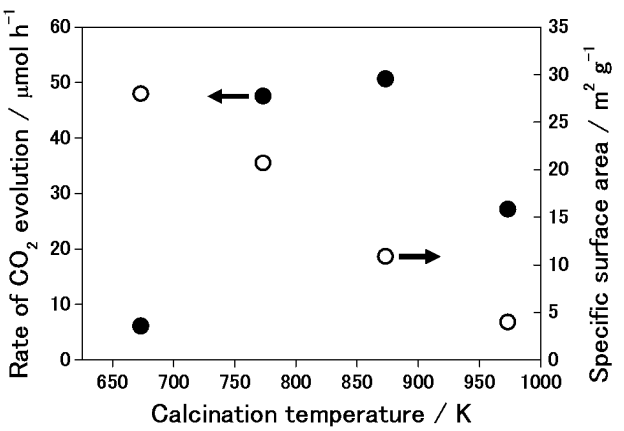

Fig. 4 Calcination temperature dependence of CO_2 generation rate (closed circles) and specific surface area (open circles) for WO_3 prepared using 180 nm PMMA (with Pt loading for CO_2 generation).

In summary, well-ordered 3DOM WO_3 was successfully prepared by a colloidal crystal template method using PMMA spheres of various diameters. The 3DOM WO_3 material thus produced has a higher specific surface area compared to WO_3 prepared without the template, and the photocatalytic activity of the Pt-loaded 3DOM WO_3 for the decomposition of acetic acid under visible light was found to be higher than that reported previously for WO_3. High-temperature calcination of 3DOM WO_3 afforded a nanoparticulate WO_3 material by sintering-induced disassembly, and this nanoparticulate material exhibited the highest photocatalytic activity for this reaction among the present samples. Further investigation of the photochemical mechanism and improvement of the catalytic activity are currently in progress.

This study was supported by the 2007 Industrial Technology Research Grant Program from the New Energy and Industrial Technology Development Organization (NEDO) of Japan.

Notes and references

‡ The photocatalytic decomposition of gaseous acetic acid was performed using a Pyrex reaction cell (internal volume, 357 mL) containing 50 mg of the photocatalyst powder spread in a 15 × 15 mm square on the cell bottom. Liquid acetic acid (1.0 μL (±5–8%), 18.0 μmol, *ca.* 1100 ppm) was then introduced into the darkened cell. After the absorption of acetic acid had reached equilibrium, the cell was irradiated with visible light ($\lambda > 400$ nm) using a 300 W xenon lamp (LX-300F, Cermax) fitted with a cutoff filter (L-42, HOYA). Components in the gas phase were analyzed by gas chromatography (Micro GC 3000A, Agilent; TCD detector) using Plot-U (for CO_2) and OV-1 (for acetic acid) columns.

1 (*a*) G. Palmisano, V. Augugliaro, M. Pagliaro and L. Palmisano, *Chem. Commun*., 2007, 3425; (*b*) M. R. Hoffmann, S. T. Martin, W. Choi and D. W. Bahnemann, *Chem. Rev*., 1995, **95**, 69.

2 (*a*) R. Asahi, T. Morikawa, T. Ohwaki, K. Aoki and Y. Taga, *Science*, 2001, **293**, 269; (*b*) T. Ohno, T. Mitsui and M. Matsumura, *Chem. Lett*., 2003, **32**, 364; (*c*) H. G. Kim, D. W. Hwang and J. S. Lee, *J. Am. Chem. Soc*., 2004, **126**, 8912; (*d*) T. Arai, M. Yanagida, Y. Konishi, Y. Iwasaki, H. Sugihara and K. Sayama, *J. Phys. Chem. C*, 2007, **111**, 7574.

3 R. Abe, H. Takami, N. Murakami and B. Ohtani, *J. Am. Chem. Soc*., 2008, **130**, 7780.

4 (*a*) S. Ikeda, N. Sugiyama, S. Murakami, H. Kominami, Y. Kera, H. Noguchi, K. Uosaki, T. Torimoto and B. Ohtani, *Phys. Chem. Chem. Phys*., 2003, **5**, 778; (*b*) B. Ohtani and S.-I. Nishimoto, *J. Phys. Chem*., 1993, **97**, 920.

5 R. C. Schroden, M. Al-Daous, C. F. Blanford and A. Stein, *Chem. Mater*., 2002, **12**, 3305.

6 B. T. Holland, C. F. Blanford, T. Do and A. Stein, *Chem. Mater*., 1999, **11**, 795.

7 J. C. Lytle, N. R. Denny, R. T. Turgeon and A. Stein, *Adv. Mater. (Weinheim, Ger.)*, 2007, **19**, 3682.

8 2 mL of commercial ammonium metatungstate solution (Nippon Inorganic Color & Chemical Co.; MW-2, 50.0 wt% as WO_3) mixed with 1 mL of methanol.

9 (*a*) M. Sadakane, T. Horiuchi, N. Kato, C. Takahashi and W. Ueda, *Chem. Mater*., 2007, **19**, 5779; (*b*) M. Sadakane, C. Takahashi, N. Kato, H. Ogihara, Y. Nodasaka, Y. Doi, Y. Hinatsu and W. Ueda, *Bull. Chem. Soc. Jpn*., 2007, **80**, 677.

10 I. M. Szilágyi, J. Madarász, G. Pokol, P. Király, G. Tárkányi, S. Saukko, J. Mizsei, A. L. Tóth, A. Szabó and K. Varga-Josepovits, *Chem. Mater*., 2008, **20**, 4116.

11 Assuming that the crystallites are spherical particles, the specific surface area is given by $6000/dA$, where d is density (monoclinic WO_3, 7.278 g cm^{-1}) and A is particle size (nm). This calculation yields specific surface areas of 0.8 and 8.2 m^2 g^{-1} for WO_3 crystals with diameters of 1 μm and 100 nm.

12 The specific surface area of 3DOM (shell structure) materials is given by $2\pi/((2 - (\pi/3))dB)$, where d is density (monoclinic WO_3, 7.278 g cm^{-1}) and B is pore diameter (nm).

13 J. N. Kondo and K. Domen, *Chem. Mater*., 2008, **20**, 835.

14 F. Li, Z. Wang and A. Stein, *Angew. Chem., Int. Ed*., 2007, **46**, 1885.